Available online at www.sciencedirect.com
ScienceDirect
Trans. Nonferrous Met. Soc. China 25(2015) 2781−2788
Transactions of Nonferrous Metals Society of China
www.tnmsc.cn

Oxidation kinetics of oxide film on bubble surface of aluminum foams produced by gas injection foaming process

Yu-tong ZHOU[1], Yan-xiang LI[1,2]

1. School of Materials Science and Engineering, Tsinghua University, Beijing 100084, China;
2. Key Laboratory for Advanced Materials Processing Technology, Ministry of Education,
Tsinghua University, Beijing 100084, China

Received 3 September 2014; accepted 2 April 2015

Abstract: In the range of 620−710 °C, air was blown into A356 aluminum alloy melt to produce aluminum foams. In order to study the influence of temperature on the thickness of oxide film on bubble surface, Auger electron spectroscopy (AES) was used. Based on the knowledge of corrosion science and hydrodynamics, two oxidation kinetics models of oxide film on bubble surface were established. The thicknesses of oxide films produced at different temperatures were predicted through those two models. Furthermore, the theoretical values were compared with the experimental values. The results indicate that in the range of 620−710 °C, the theoretical values of the thickness of oxide film predicted by the model including the rising process are higher than the experimental values. While, the theoretical values predicted by the model without the rising process are in good agreement with the experimental values, which shows this model objectively describes the oxidation process of oxide film on bubble surface. This work suggests that the oxidation kinetics of oxide film on bubble surface of aluminum foams produced by gas injection foaming process follows the Arrhenius equation.

Key words: aluminum foam; gas injection foaming process; oxide film; oxidation kinetics

1 Introduction

Researches on gas injection foaming process started from the end of 1980s [1]. Compared with other methods, gas injection process possesses some advantages such as low cost and the capability of continuous production. Its products can be processed as aluminum foam sandwiches and aluminum foam bricks, which are new materials used in the fields of impact resistance and energy absorption [2]. Nonetheless, a huge progress has been already made in a series of technical problems [1,3], and the issue of foam stability has been still under a lot of controversies until now. Although opinion varies from people to people, most researchers believe that the oxidation of bubble surface and the attachment of particles existing in the melt to the bubble surface are essential for foam stability. Therefore, the stabilization of foams is caused by at least two mechanisms, the segregation of particles to the interface and the oxide film covering the bubble surface [4].

In the past 20 years, the effects of particles on foam stability have become a hot topic. The relationships between wetting behavior, distribution of particles and foam stability were investigated deeply [5−8]. The possible effects of particles in stabilizing foams could be increasing viscosity, decreasing surface tension, modulating the interface and bridging between interfaces. However, the researches related to the effects of oxide film are less. We only know that the stability of foams with oxide film is much better than that of foams without oxide film [9]. Almost nobody has studied the oxidation kinetics of oxide film so far, which leads to the result that the understanding of the role of oxide film on bubble surface in foam stability is relatively superficial. Only BABCSÁN et al [9] analyzed the relationship between the thickness of oxide film and isothermal holding time at 680 °C. But they have not studied the oxidation kinetics deeply. Actually, the cognitions of the oxidation kinetics of directed melt oxidation process of Al−Si−Mg alloys are very profound at present, since the studies of preparation of MMC by directed melt oxidation method

---

Foundation item: Project (51371104) supported by the National Nature Science Foundation of China
Corresponding author: Yan-xiang LI; Tel: +86-10-62773640; E-mail: yanxiang@tsinghua.edu.cn
DOI: 10.1016/S1003-6326(15)63903-6

were very popular in 1980s [10,11]. This has laid a good foundation for the study of oxidation kinetics of oxide film. VLACH et al [12] studied the process of directed melt oxidation and suggested that the nominal activation energy of Al−Si−Mg alloy in the range of 1100−1300 °C was about 270 kJ/mol. Based on theoretical calculation, ZHOU et al [13] found that the nominal activation energy of aluminum alloy decreased significantly with the increase of Si content. When the content of Si was more than 7% (mass fraction) and the content of Mg was less than 1% (mass fraction), the nominal activation energy would decrease to be less than 100 kJ/mol. But the process of gas injection foaming method is special, the bubbles keep moving when they are in the melt. Whether the oxidation kinetics of oxide film of aluminum foams is consistent with that of directed melt oxidation process or not is still unknown. Our previous study showed that oxygen volume fraction of foaming gases had little effect on the thickness of oxide film [14], which was in agreement with NAGELBERG’s work [15]. However, there are still some differences existing in the thickness of oxide film between our previous work and BABCSÁN’s work [16]. Therefore, further studying the oxidation process of oxide film on bubble surface and identifying the factors that control the formation of oxide film on bubble surface should be tasks of top priority. It is impossible for us to explain the distinctions between different experimental results scientifically and understand the effects of oxide film in improving foam stability before the above problems are solved. Obviously, this study of the influence of temperature on the thickness of oxide film on bubble surface can help us not only gain a further scientific understanding of foam stability, but also improve the gas injection foaming process technique.

2 Experimental

The raw material used to produce aluminum foams was A356 aluminum alloy. 10% Al_2O_3 (volume fraction) particles, with an average size of 10 μm, were mixed into A356 aluminum alloy melt as foam stabilizer and fully dispersed by mechanical stirring. The orifice diameter of nozzle was about 0.5 mm, foaming depth (the distance between the nozzle and the surface of the melt) was 15 cm and the gas flow rate was 0.9−1.0 L/min. The gas chosen for foaming was compressed air, which was supplied by a professional manufacturer. 620−710 °C is a relative common temperature range for aluminum foam preparation. Accordingly, gas was blown into the formable precursor to prepare aluminum foams at 620, 650, 680 and 710 °C through an experimental platform built by ourselves [17]. Since the melt is enough, the changes of foaming depth during the preparation process of aluminum foams can be neglected. Besides, in order to control the oxidation time, aluminum foams were removed from the melt surface in 40 s.

The average thickness of cell walls was measured with the help of an image analysis software developed by our laboratory. More than 10 cell wall specimens produced under each experimental condition were selected to ensure the accuracy of the final results. In order to determine the thickness of oxide film on bubble surface, several cell wall specimens were randomly cut from aluminum foams and cleaned by ultrasonic. After that, these specimens were analyzed on a PHI−700 Auger electron spectroscope. The analyses only focused on the mole fraction of Al and O (regarding the total number of atoms of these two elements as 100%). Two or three cell walls of aluminum foams produced under each experimental condition were selected as analysis objects. The average composition of these specimens was regarded as the result.

3 Results and discussion

3.1 AES depth profiles of oxide films on bubble surface

Aluminum foam samples were processed by an electric discharging cutting machine and then scanned to acquire their vertical section images. A typical vertical section of aluminum foam produced at 680 °C is shown in Fig. 1. The average cell size measured by line method was 13.5−14.5 mm and the relative density of aluminum foam was 0.07−0.08. Cell wall specimens were observed with the help of SEM. A typical SEM microstructure of cell wall specimen is shown in Fig. 2. Obviously, all the cell wall surfaces are covered with an oxide film completely and almost no particle absorbs to the interface of cell wall, suggesting that the added Al_2O_3 particles will not interfere with the results of AES experiment. Moreover, according to the statistical results, the average thickness of cell walls is about 100 μm.

Fig. 1 Typical vertical section of aluminum foams produced at 680 °C

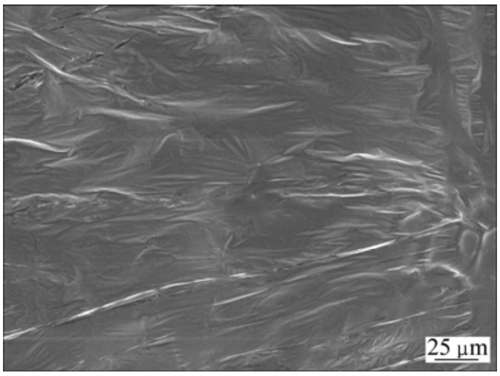

Fig. 2 Typical SEM microstructure of cell wall produced at 680 °C

AES depth profiles of oxide films on bubble surface of aluminum foams produced at different temperatures are shown in Fig. 3. The distributions of two kinds of elements Al and O were measured along the direction of oxide film thickness. Comparing the AES depth profiles, it can be found that these two composition curves have a tendency to move right with the increase of temperature. With etching, the tendencies of two curves are not identical. Namely, the composition of O decreases gradually and that of Al increases slowly. All the curves tend to be stable eventually. We can infer from the experimental result that the oxide film on bubble surface is penetrated gradually. In this sense, the elemental concentration transits from the composition of oxide film to that of A356 aluminum alloy. Because mole fractions of O atom in Al_2O_3, MgO and $MgAl_2O_4$ (the main compositions of the oxide film of A356 aluminum alloy [12,18]) are all located in the range of 50%−60%, we think that the oxide film on bubble surface is penetrated when the O atom content decreases to be less than 60%. As can be seen from Table 1, the thicknesses of oxide films on bubble surface of aluminum foams produced at 620, 650, 680 and 710 °C are 11.9, 12.4, 14.3 and 16.7 nm, respectively. Obviously, the thickness of oxide film on bubble surface increases with the increase of temperature.

3.2 Oxidation kinetics model of oxide film on bubble surface

According to the knowledge of corrosion science and experimental results [18], the directed melt oxidation process of A356 aluminum alloy follows a parabolic law, which is shown as follows [19]:

$$(\Delta m)^2 = k_p t \tag{1}$$

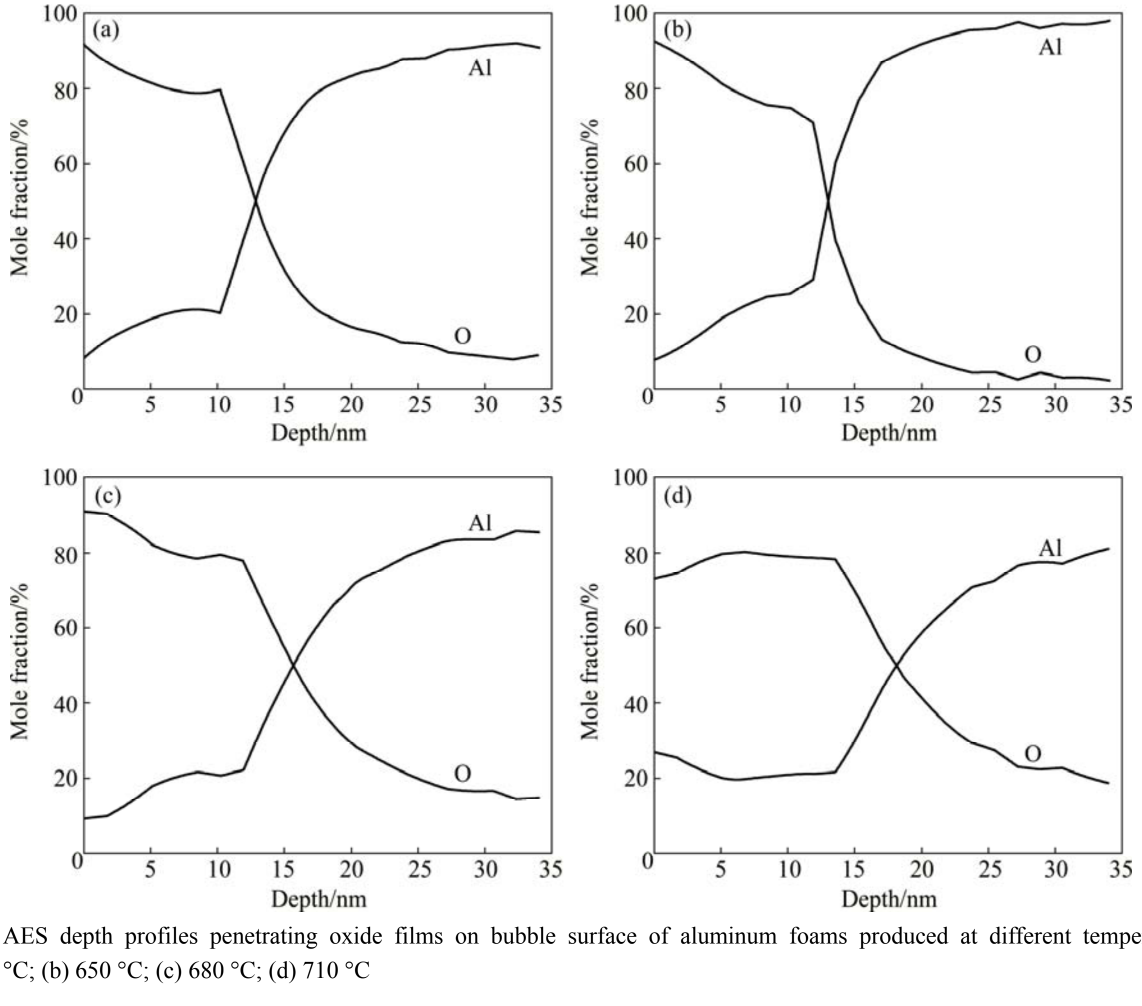

Fig. 3 AES depth profiles penetrating oxide films on bubble surface of aluminum foams produced at different temperatures: (a) 620 °C; (b) 650 °C; (c) 680 °C; (d) 710 °C

Table 1 Thicknesses of oxide films on bubble surface of aluminum foams produced at different temperatures

Temperature/°C	620	650	680	710
Thickness/nm	11.9	12.4	14.3	16.7

where Δm is the mass gain by oxidation, k_p is the parabolic constant, and t is the oxidation time. With the increase of oxidation temperature, the diffusion coefficients of metal atoms and non-metal atoms increase. So, the parabolic constant k_p will be enhanced to a certain extent and the oxidation process will be accelerated as well. The relationship between parabolic constant and temperature can be expressed by Eq. (2) (Arrhenius equation) [19]:

$$k_p = A\exp\left(-\frac{E_a}{RT_m}\right) \tag{2}$$

where A is a constant, E_a is the nominal activation energy, R is the mole gas constant and T_m is temperature. Using logarithm function on both sides of Eq. (2) yields Eq. (3):

$$\ln k_p = \ln A - \frac{E_a}{RT_m} \tag{3}$$

As the nominal activation energy E_a remains unchanged in a certain range of temperature, its value can be determined by the slope of curve of ln k_p vs T_m^{-1}.

The data of thermo gravimetric experiment of A356 aluminum alloy carried out at 690 and 730 °C are shown in Fig. 4 [20]. As can be seen from Fig. 4, the slopes of those two fitting lines are their own parabolic constants according to Eq. (1). In the range of 690−730 °C, we can draw the relationship between lg k_p and T_m^{-1} as Fig. 5. According to Eq. (3), the slope of the fitting line in Fig. 5 is $-E_a/(R\ln 10)$. Thus, the nominal activation energy of A356 aluminum alloy is E_a=87.3 kJ/mol.

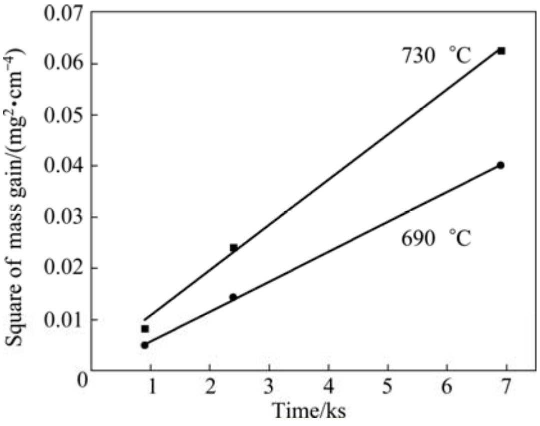

Fig. 4 Relationship between $(\Delta m)^2$ and oxidation time of A356 aluminum alloy

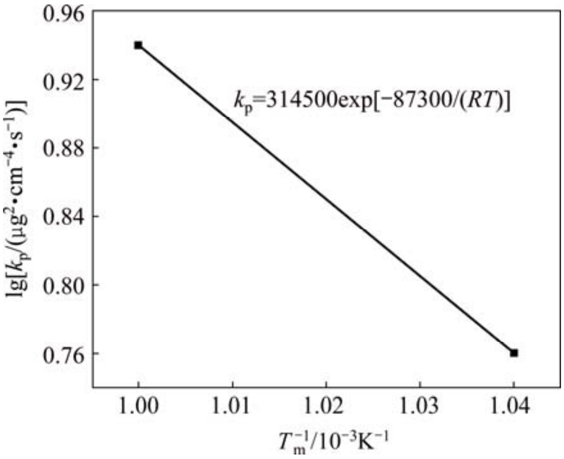

Fig. 5 Relationship between lg k_p and T_m^{-1} of A356 aluminum alloy

The process of gas injection foaming method is relatively special. At first, the bubbles form at the orifice of a nozzle, and then they detach the nozzle and rise to the surface of the melt. After that, foams accumulate there and solidify finally. Because the diffusion velocity of atoms decreases significantly after the cell wall solidifies, we consider that the oxidation mainly happens before the cell walls solidify. Thus, the oxidation time t probably contains the following two parts: the time t_a begins from the bubble forming at the nozzle to rising to the surface of the melt and the time t_b needed for the cell walls to cool from high temperature to the liquidus. Based on the research on bubble formation at a submerged orifice conducted by FAN et al [17], the time from bubbles forming at the orifice to detaching the nozzle is approximately 0.03 s. So, this period of time can be ignored. In this sense, t_a approximately equals the time of bubble rising process. Since the oxidation behavior of bubbles during the rising process is not well understood, a model including the rising process ($t=t_a+t_b$) and a model without the rising process ($t=t_b$) are both established to predict the thickness of oxide film.

In order to estimate the time of bubble rising process accurately, the motion process of bubbles must be profoundly studied. The bubbles with a diameter of 14 mm cannot remain sphere during their rising process. Affected by water pressure and other factors, the shape of bubbles will change to ellipsoid or spherical-cap when they rise. So, the assumption of regarding the bubbles as rigid spheres is not applicable to this system. In other words, the rising velocity cannot be obtained by the calculation equations based on Newtonian system [21].

DAVIS and TAYLOR [22] studied the mechanics of large bubbles rising through water (the dynamic viscosity of water at 20 °C is 1.01 mPa·s). They thought that the shape of bubble would become spherical-cap in the rising process. Based on the experiments carried out in water at 20 °C, TALAIA [23] modified the achievements made by the predecessors. He proposed that the surface tension and viscosity were negligible when the equivalent diameter of bubbles was larger than 13 mm and the relationship between the terminal velocity and the equivalent diameter of bubble could be expressed as

$$v=\left(0.694\pm 0.021\right)\left[\frac{gd(\rho_\mathrm{l}-\rho_\mathrm{g})}{\rho_\mathrm{l}}\right]^{\frac{1}{2}} \tag{4}$$

where v is the terminal velocity of bubble rising process, g is the gravitational acceleration, d is the diameter of bubbles, ρ_l and ρ_g are the densities of the melt and compressed air.

At 690 °C, the dynamic viscosity of A356 aluminum alloy is about 1.05 mPa·s [24]. The influence of ceramic particles on the dynamic viscosity of the melt can be described as [25]

$$\mu_\mathrm{r}=\left[1+2.5\varphi+10.05\varphi^2+0.00273\exp\left(16.6\varphi\right)\right]\mu_\mathrm{f} \tag{5}$$

where μ_r is the apparent viscosity of the melt after adding particles, μ_f is the original viscosity of the melt and φ is the volume fraction of added ceramic particles. As can be seen from Eq. (5), adding 10% (volume fraction) ceramic particles will increase the viscosity of the melt by 40% approximately. Unlike the process of melt changing from liquid to semi-solid, no magnitude variation of viscosity will be caused by the added particles. Therefore, we can use Eq. (4) to estimate the terminal velocity of bubbles rising in the A356 aluminum alloy melt. During the rising process, bubbles will experience an accelerated process before they reach the terminal velocity. However, for the bubbles with a diameter of 14 mm, the time of accelerated motion stage is very short [26]. Consequently, this period of time can be ignored as well. Accordingly, the bubble rising process can be considered as a steady motion process when we calculate the bubble rising time (Eq. (6)):

$$t_\mathrm{a}=\frac{s}{v} \tag{6}$$

where s is foaming depth. Based on the actual experimental conditions, the calculated rising time of the bubbles with a diameter of 14 mm is around 0.58 s. Then, the relationship between the mass gain by oxidation and temperature during the bubble rising process can be obtained.

Cooling process starts immediately when the bubbles rise to the surface of the melt. Due to the complex structure of aluminum foams, there is still no model that can describe the cooling process of aluminum foams accurately. So, the cooling process is studied through a simple cell wall model in this paper (Fig. 6(a)). For the convenience of calculation, the cell wall model is simplified as a cube with length, width and height of 1 cm, 100 μm and 1 cm, respectively (as shown in Fig. 6(b)).

According to the gas flow rate, the average cell size and the cross section area of aluminum foams, it can be calculated that 2−2.5 s is needed for the bubbles to form a full layer of aluminum foam. Based on this result, an assumption can be made that when a bubble rises to the surface of the melt, the temperature of upper foams contacting with this bubble approximately equals the liquidus temperature (615 °C). Under the cooling conditions of aluminum foams, heat conduction and thermal radiation are the main modes of heat loss. While the effect of convection is much lower than that of heat conduction or thermal radiation. Heat conduction mainly occurs between the upper foams with lower temperature and the cell wall. The upper foams cool down the cell wall through Face 1. The heat flow of heat conduction under steady condition can be calculated by

$$\varphi_a=A_1q=\frac{A_1\lambda\left[\left(\frac{T_1+T_\mathrm{m}}{2}\right)-T_2\right]}{\delta} \tag{7}$$

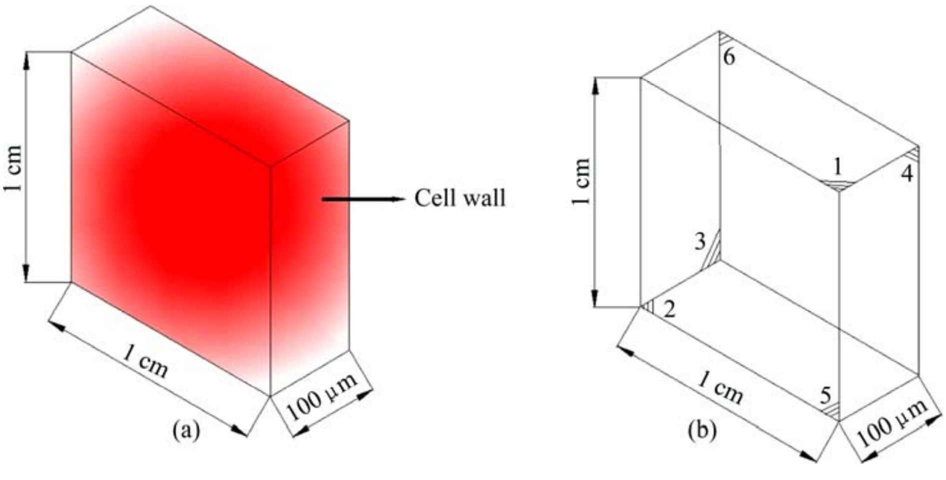

Fig. 6 Schematic diagram of cell wall cooling model: (a) Cell wall model; (b) Number of cell wall surfaces

where φ_a is heat flow of heat conduction, A_1 is the area of Face 1, λ is the thermal conductivity of liquid A356 aluminum alloy (about 80 W/(m·°C) [27]), T_l is the liquidus temperature of A356 aluminum alloy, T_m is the temperature of the melt, T_2 is the temperature of upper foams, δ is the average distance of heat transfer. In addition to heat conduction, the cell wall can also radiate heat through Faces 5 and 6. The heat flow of thermal radiation during the cooling process can be expressed as

$$\varphi_b = \frac{A_5 C_b \left[\left(\frac{T_l + T_m}{200} \right)^4 - \left(\frac{T_2}{100} \right)^4 \right]}{\frac{2}{\varepsilon} - 1} \tag{8}$$

where φ_b is heat flow of thermal radiation, A_5 is the area of Face 5, C_b is blackbody radiation coefficient, ε is the emissivity of the cell wall. The emissivity of metals increases with the increase of temperature. In the range of 620−710 °C, the emissivity of smooth aluminum plates is 0.6−0.7 [28]. The emissivity of A356 aluminum alloy should be close to that of pure aluminum, so, the value of emissivity is regarded as 0.65 in calculation. Since the faces connected to Faces 3 and 4 are the other cell walls of the same bubble, the temperature of these cell walls is regarded as being always equal to that of the cell wall under studying during the cooling process. In other words, no heat exchange occurs through Faces 3 and 4. For a 100 μm-thick cell wall, the heat loss before its temperature reaches liquidus is shown as Eq. (9):

$$Q = \frac{A_5 x p_l}{M} c_p (T_m - T_l) \tag{9}$$

where Q is the heat loss, x is the average thickness of cell walls, M is the molar mass of A356 aluminum alloy and c_p is specific heat capacity of A356 aluminum alloy at constant pressure. Neglecting the influence of convection, the time needed for the liquid metal within a cell wall to cool from high temperature to liquidus can be calculated by

$$t_b = \frac{Q}{(\varphi_a + 2\varphi_b)} \tag{10}$$

The results show that regardless of the preparation temperature, t_b is always about 2 s. This value is similar to the time needed for the bubbles to form a full layer of foams, which proves the former assumption that the temperature of upper foams is approximately 615 °C is reasonable. Moreover, it also indicates that the cooling process described by the oxidation kinetics model can be continuous in the preparation of aluminum foams.

On the basis of t_b and the already acquired relationship between the mass gain by oxidation and temperature during the bubble rising process, regarding $(T_l+T_m)/2$ as the qualitative temperature, the mass gains by oxidation of the model including the rising process and the model without the rising process can be calculated respectively with the help of Eqs. (1) and (2).

3.3 Comparison between theoretical results and experimental results of thickness of oxide film on bubble surface

A356 aluminum alloy contains a variety of alloy elements and its oxidation process is significantly influenced by Mg and Si. As a result, the composition and structure of the oxide film of A356 aluminum alloy is more complicated than those of oxide film of pure aluminum. VLACH et al [12] found that the structure of oxide film of Al−Si−Mg alloy could be divided into three layers. From the outside to the inside, the compositions were MgO, $MgAl_2O_4$ and Al_2O_3, respectively. LIM et al [18] found that the surface layer of oxide film of A356 aluminum alloy was mainly composed of MgO. Other compositions like $MgAl_2O_4$ and Al_2O_3 would not appear until a certain depth. Although the accurate composition of oxide film on bubble surface cannot be determined, the densities and mass fractions of O in MgO, $MgAl_2O_4$ and Al_2O_3 are relatively similar. So, the composition of oxide film on bubble surface has little effect on the estimated thickness of oxide film. For the convenience of calculation, the density and the mass fraction of O in oxide film on bubble surface are regarded as the average values of those of MgO and Al_2O_3. Namely, the parameters are 3.8 g/cm^3 and 43%, respectively. Based on the already known relationship between the mass gain by oxidation and temperature, the thickness of oxide film on bubble surface estimated by two kinds of models can be calculated by

$$h = \frac{\Delta w}{w_O \rho_f} \tag{11}$$

where h is the thickness of oxide film on bubble surface, ρ_f and ω_O are the density and the mass fraction of O in oxide film.

The calculated results of the thickness of oxide film are compared with the experimental results (Fig. 7). In the range of 620−710 °C, the theoretical values of the thickness of oxide film predicted by the model including the rising process are much higher than the experimental values. However, the theoretical values of the thickness of oxide film predicted by the model without the rising process are only higher than the experimental values by 1−2 nm. Both of them agree well with each other. Precisely, with the increase of temperature, theoretical values and experimental values both increase. In addition, the rates of the increase are also similar. The differences between the results predicted by those two kinds of models and the experimental results suggest that the estimated oxidation rate or oxidation time is probably a little higher. Moreover, although oxide film will certainly form on the bubble surface during the bubble rising process, the oxidation time of cell wall's cooling process is much longer, so the latter one should be the main part of the whole oxidation process of oxide film on bubble surface. Though, we did not take the oxidation process of oxide film during the solidification process of cell wall into account, it is proved that the oxidation kinetics model of oxide film on bubble surface established in this paper grasps the main factors and objectively describes the real oxidation process. Overall, the relationship between the thickness of oxide film on bubble surface and temperature conforms to the predictions of Eq. (11), indicating that the oxidation kinetics of oxide film on bubble surface of aluminum foams produced by gas injection process follows the Arrhenius equation.

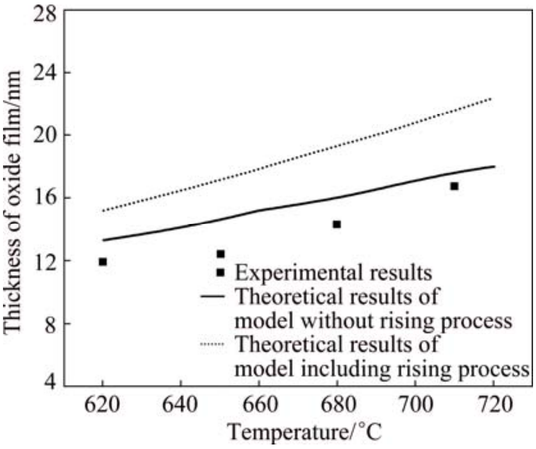

Fig. 7 Comparison between theoretical and experimental results of thickness of oxide film on bubble surface

4 Conclusions

1) The thickness of oxide film on bubble surface increases from 11.9 to 16.7 nm, when temperature increases from 620 to 710 °C, which confirms that the thickness of oxide film of aluminum foams produced by gas injection foaming process increases with the increase of temperature.

2) In the range of 620−710 °C, the theoretical values of the thickness of oxide film predicted by the model including the rising process are much higher than the experimental values. However, the theoretical values predicted by the model without the rising process and the experimental values have little difference. This study indicates that the oxidation kinetics of the oxide film on bubble surface follows the Arrhenius equation.

3) This study defines the factors controlling the oxidation process of oxide film on bubble surface and builds a good foundation of further research on the role of oxide film in stabilizing metal foams.

References

[1] BANHART J. Manufacture, characterization and application of cellular metals and metal foams [J]. Progress of Materials Science, 2001, 46(6): 559−632.

[2] ZU Guo-yin, LU Ri-huan, LI Xiao-bing, ZHONG Zhao-yang, MA Xing-jiang, HAN Ming-bo, YAO Guang-chun. Three-point bending behavior of aluminum foam sandwich with steel panel [J]. Transactions of Nonferrous Metals Society of China, 2013, 23(9): 2491−2495.

[3] LEFEBVRE L P, BANHART J, DUNAND D C. Porous metals and metallic foams: Current status and recent developments [J]. Advanced Engineering Materials, 2008, 10(9): 775−787.

[4] BANHART J. Light-metal foams — History of innovation and technological challenges [J]. Advanced Engineering Materials, 2013, 15(3): 82−111.

[5] BANHART J. Metal foams: Production and stability [J]. Advanced Engineering Materials, 2006, 8(9): 781−794.

[6] HAIBEL A, RACK A, BANHART J. Why are metal foams stable [J]. Applied Physical Letter, 2006, 89: 154102−154104.

[7] BABCSÁN N, LEITLMEIER D, BANHART J. Metal foams-high temperature colloids. Part I: Ex situ analysis of metal foams [J]. Colloid and Surface A, 2005, 261: 123−130.

[8] SHEN P, FUJII H, MATSUMOTO T, NOGI K. Wetting of (0001) α-Al_2O_3 single crystals by molten Al [J]. Scripta Materialia, 2003, 48: 779−784.

[9] BABCSÁN N, LEUTLMEIER D, DEGISCHER H P, BANHART J. The role of oxidation in blowing particle-stabilized aluminum foams [J]. Advanced Engineering Materials, 2004, 6(6): 421−428.

[10] MURTHY V S R, RAO B S. Microstructural development in the directed melt-oxidized (DIMOX) Al−Mg−Si alloys [J]. Journal of Materials Science, 1995, 30: 3091−3097.

[11] NEWKIRK M S, URQUHART A W, ZWICHER H R. Formation of Lanxide ceramic composite materials [J]. Journal of Materials Research, 1986, 1(1): 81−89.

[12] VLACH K C, SALAS O, NI H, JAYARAM V, LEVI C G, MEHRABIAN R. A thermogravimetric study of the oxidation of Al_2O_3/Al alloy composites [J]. Journal of Materials Research, 1991, 6(9): 1982−1995.

[13] ZHOU Xi-ya, SHEN Yu-hui, CHEN Jian-feng, GAO Qin. Study on the dynamics of oxidation growth of Al_2O_3/Al composites [J]. Acta Materiae Compositae Sinica, 1997, 14(3): 9−14. (in Chinese)

[14] ZHOU Yu-tong, LI Yan-xiang. Oxide film on bubble surface of aluminum foams produced by gas injection foaming process [J]. Transactions of Nonferrous Metals Society of China, 2015, 25(7): 2429−2437.

[15] NAGELBERG A S, STANISLAV A, URQUHART A W. Formation of Al_2O_3/metal composites by the directed oxidation of molten aluminum-magnesium-silicon alloy. Part II: Growth kinetics [J]. Journal of American Ceramic Society, 1992, 75(2): 455−462.

[16] BABCSÁN N, LEITLMEIER D, DEGISCHER H P. Foamability of particle reinforced aluminum melt [J]. Materialwissenschaft und Werkstofftechnik, 2003, 34: 22−29.

[17] FAN Xue-liu, CHEN Xiang, LIU Xing-nan, ZHANG Hui-ming, LI Yan-xiang. Bubble formation at a submerged orifice for aluminum foams produced by gas injection method [J]. Metallurgical and Materials Transaction A, 2013, 44: 729−737.

[18] LIM S C, KIM D H, KIM J S, LEE C H, YOON E P. Decomposition kinetics of machining oil and oxidation of A356.2 aluminium alloy in aluminium recycling process [J]. Materials Science and Technology, 1997, 13(10): 859−864.

[19] KOFSTAD P. High temperature corrosion [M]. London: Elsevier Applied Science Publishers Ltd., 1988.

[20] MIRESMAEILI S M. Effect of strontium on the oxidation behavior of liquid Al−7Si alloy [J]. Oxidation of Metals, 2009, 71: 107−123.

[21] CHEN Wen, ZHOU Xiao-de, GUO Jin-long, LI Hua. Experimental study of the velocity of bubble rising in water [J]. Journal of Xi'an University of Technology, 2000, 16(1): 57−60. (in Chinese)

[22] DAVIS R M, TAYLOR G. The mechanics of large bubbles rising through extended liquids and through liquids in tubes [J]. Proceedings of the Royal Society: Mathematical, Physical and Engineering Science, 1950, 200: 375−390.

[23] TALAIA M A R. Terminal velocity of a bubble rise in a liquid column [J]. International Journal of Physical, Nuclear Science and Engineering, 2007, 1(4): 12−16.

[24] WANG D, OVERFELT R A. Oscillating cup viscosity measurements of aluminum alloys: A201, A319 and A356 [J]. International Journal of Thermophysics, 2002, 23(4): 1063−1076.

[25] THOMAS D G. Transport characteristics of suspension: VIII. A note on the viscosity of Newtonian suspensions of uniform spherical particles [J]. Journal of Colloid Science, 1965, 20(3): 267−277.

[26] ZUO Juan-li, TIAN Wen-xi, QIU Sui-zheng, CHEN Rong-hua, SU Guang-hui. Numerical simulation on single bubble rising behavior in liquid metal using moving particle semi-implicit method [J]. Atomic Energy Science and Technology, 2011, 45(12): 1449−1455. (in Chinese)

[27] SU Da-wei, ZHAO Yu-tao. Simulation of filling and solidification of aluminum alloy wheel in low pressure die casting [J]. Special Casting & Nonferrous Alloys, 2007, 27(9): 682−684. (in Chinese)

[28] LIU Yu-fang, HU Zhuang-li, SHI De-heng. Normal emissivity of aluminum at different temperature measured by double-light-path contrast measurement technique [J]. Optical Technique, 2009, 35(S1): s90−s92. (in Chinese)

吹气法泡沫铝泡壁表面氧化膜氧化动力学

周宇通[1]，李言祥[1,2]

1. 清华大学 材料学院，北京 100084；
2. 清华大学 先进成型制造教育部重点实验室，北京 100084

摘　要：在 620~710 °C 范围内，将压缩空气吹入含有陶瓷颗粒的 A356 铝合金熔体中制备泡沫铝样品。运用 AES 技术对泡壁表面进行分析，以研究温度对表面氧化膜厚度的影响。根据金属腐蚀学及流体力学原理建立表面氧化膜泡壁氧化动力学模型。从理论上预测不同温度条件下泡沫铝泡壁表面氧化膜的厚度，并与实验值进行对比。结果表明，在 620~710 °C 范围内，考虑上浮过程的模型预测的氧化膜厚度理论值明显高于实验值，而不包含上浮过程的模型预测的理论值与实验值符合较好，且后者能更好地描述泡沫铝泡壁表面氧化膜的氧化过程。研究表明，吹气法泡沫铝泡壁表面氧化膜的氧化速率与温度之间的关系符合 Arrhenius 公式。

关键词：泡沫铝；吹气法；氧化膜；氧化动力学

(Edited by Wei-ping CHEN)